Hindawi
Journal of Nanomaterials
Volume 2022, Article ID 4848864, 14 pages
https://doi.org/10.1155/2022/4848864

*Research Article*

# Fractional Analysis of Dissipative Viscous Fluid Flow with Mixed Convection and Variable Viscosity

**Abir Mouldi,[1] Riadh Marzouki,[2] Mohamed Hechmi El Ouni,[3] and Abdul Bariq[4]**

[1]*Department of Industrial Engineering, College of Engineering, King Khalid University, Abha-61421, Saudi Arabia*
[2]*Department of Chemistry, College of Science, King Khalid University, Abha-61421, Saudi Arabia*
[3]*Department of Civil Engineering, College of Engineering, King Khalid University, Abha-61421, Saudi Arabia*
[4]*Department of Mathematics, Laghman University, Mehterlam, 2701 Laghman, Afghanistan*

Correspondence should be addressed to Abdul Bariq; abdulbariq.maths@lu.edu.af

Received 29 September 2021; Accepted 21 February 2022; Published 6 April 2022

Academic Editor: Hui Yao



Time-dependent viscosity and thermal conductivity have been studied in relation to flow and thermal energy propagation along a vertical turning cone. Except the density variance, the other fluid's properties are assumed to be constant. Using the similarities procedure, the nonlinear system of differential equations is simplified to dimensionless ODEs. The resultant nonlinear ODEs system is computed while using fractional code FDE12, and the findings are quantitatively examined using the bvp4c approach for accuracy and consistency. In form of figures and tables, the behavior of momentum, energy, and mass is interpreted versus the physical constraints. The axial and radial velocity, both declines with the variation of unsteadiness parameter $S$. The axial velocity of the fluid is considerably increased when the mixed convection parameter is elevated, but the radial velocity is reduced. Similarly, when the variable viscosity increases, the velocity profile develops.

## 1. Introduction

The results of this study show that disk-cone appliances are used in a variety of technical applications, including determining the viscosity of a fluid (viscosimetry), convective diffusion, medical devices, and biomedicine for oxygen measurement [1]. The heat transfer through a spinning cone is also addressed in this research. Many academics are drawn to this sort of study to investigate its properties, behavior, and applications. Turkilmazoglu [2] investigated a steady Newtonian viscous fluid over a rotating cone using the homotopy analysis technique. The mixed convective simulation with momentum and heat distribution across a perforated upward spinning cone in an ambient liquid was numerically calculated by Chamkha and Al-Mudhaf [3]. They hypothesized that when cone angular velocity varies, axial, and tangential velocity increases considerably. Garrett et al. [4] investigated the fluid flow across a turning cone (half angle) in axial direction. The MHD (magnetohydrodynamics) nanoliquid flow with Brownian motion and thermophoresis influence over a revolving cone was deled by Nadeem and Saleem [5] and Towers and Garrett [6]. It is worth noting that surface temperature and Mach number destabilise the system, whereas suction stabilises it. Hayat et al. [7] used a shooting method to emphasize the MHD chemical reactivity of an unsteady viscous fluid over a turning cone. Chamkha et al. [8] evaluated the influence of a rotating cone on a 3D CNT hybrid nanofluid in a trapezoid permeable cavity, considering MHD interactions.

The upshot of unsteady viscosity on viscous fluid characteristics causes some variation. The viscosity of liquids, for example, decreases as temperature goes up, but the viscosity of gases improves. The rises in thermal energy cause friction in oily fluids, which affects fluid viscosity, and the viscosity no longer holds consistent. In light of this deficiency, a growing number of researchers are focusing their efforts on demonstrating the impact of changing viscosity phenomena under various situations. The effects of fluctuating viscosity

of third-grade dispersed fluid flow via a conduit have been explored by Christie and Massoudi [9]. The numerical outputs were discovered using the finite difference method. Seddeek [10] investigated unstable free convection MHD flow across an infinite plate under the influence of a magnetic field and changing viscosity. The computational solution of the simulated equations is done using the finite difference method. MHD boundary layer flow over an extending heated surface with variable viscosity is reported by Pantokratoras [11]. Their analysis also included a graphical representation of viscosity variations. Mukhopadhyay and Layek [12] looked studied heat exchange across a stretched vertical porous surface with changing fluid viscosity. They discovered that increasing the viscosity, enhances the velocity while decreasing the energy field. Using a discrete variant of HAM known as spectral homotopy evaluation over a stretched surface, Dada and Onwubuoya [13] addressed mass and energy distribution through fluid flow with changing viscosity and activation energy. Hazarika et al. [14] evaluated the upshots of changing viscosity, thermal radiation, and MHD on fluid flow through a vertical cone.

The thermal transition rates are affected by viscous dissipation, which acts as an energy source. The relevance of viscous dissipation is determined by whether the cone is freezing or warmed. Reddy et al. [15] estimated MHD flow and energy propagation across a stretched substrate as a function of heat source and viscous dissipation. Mabood et al. [16] evaluated the MHD flow, energy transport, and chemical reaction of a nanofluid containing copper Cu and aluminium oxide particulates in a porous media under the viscous dissipation influence. Deebani et al. [17] assessed the role of viscous dissipation and MHD across a revolving cone. Gayatri et al. [18] studied viscous dissipation in 2D fluid flow with varying thickness and slip coefficients across a stretched surface. They discovered that the slip parameters increase friction while lowering fluid velocity. Using the Atangana-Baleanu fractional method, Saqib et al. [19] investigated electro-osmotic nanofluid flow.

Fractional calculus, which is an extension of regular calculus, has a 300-year history. This field has exploded in popularity in recent years. Almost all activities in applied sciences are described by signal processing, fluid flow in permeable substances, wave transference in mechanical properties, finance theory, and biological system electric conductance [20, 21]. Many definitions exist for the fractional derivative; however, the Caputo and Riemann Liouville fractional derivatives are particularly important in terms of applicability [22]. We know that the kernel was single in both fractional definitions. To overcome this difficulty, Caputo and Fabrizio presented a new point of view of noninteger order derivative with nonsingular kernel [23] in 2016, which is highly beneficial for a variety of physical problems. Manzoor et al. [24] analyzed the uniqueness and existence of solutions of fractional order differential equations with Caputo derivatives. They came up with a set of requirements to assure solution validity while maintaining Hyers-Ulam stability. The fractional assessments for Darcy hybrid nanoliquid flow over a perforated spinning disc were elaborated by Li et al. [25]. The proposed model has been put up using Matlab fractional code Fde12 to produce the fractional solution. The outputs are compared to the fast-approaching numerical Matlab scheme boundary value solver for correctness and validity of the resultant framework.

We generalized the approach of [26] based on the aforementioned literature and its application in the actual world. The goal of this study is to assess the upshots of time-dependent viscosity on flow, thermal energy, and mass transfer in a vertical rotating cone. The spinning phenomenon is arranged in the format of a system of PDEs for this reason. Which are solved using the fractional code FDE12, and the results are checked for validity and correctness using the Matlab numerical software boundary value solver (bvp4c). The findings are depicted graphically and shortly reviewed.

## 2. Mathematical Formulation

We considered axisymmetric, an incompressible and unsteady fluid flow with an angular velocity $\Omega$ across a rotating cone. The $u$, $v$, and $w$ are the velocity component has been considered along $x$, $y$, $z$ direction. The gravity $g$ impact is downward, and the buoyancy force exist due to the temperature variation. The tangential direction influences temperature $T_w$variability near the cone's edge, while temperature $T_\infty$ away from the cone kept fixed. Fluid flow mechanism over a rotating cone is depicted through Figure 1. Furthermore, the variable thermal conductivity and viscosity are expressed as [26]: the variable viscosity model used here is the Reynold's model. The Taylor series expansion has been used to obtain.

$$\begin{aligned} \mu &= \mu_0(1 - A\theta), \mu = \mu_0 e^{-\eta(T-T_\infty)}, \\ k &= k_0 e^{-c(T-T_\infty)}, k = k_0(1 - \varepsilon\theta). \end{aligned} \tag{1}$$

Where

$$A = (T_w - T_\infty)\eta \text{ and } \varepsilon = -(T_w - T_\infty)c. \tag{2}$$

Here, $k_0$ and $\mu_0$ is the fluid conductivity and dynamic viscosity.

The governing system of nonlinear PDEs for momentum, mass, and energy may be written as by utilising Boussinesq approximation boundary layer theory and the aforementioned assumption [26]:

$$\frac{\partial(xu)}{\partial x} + \frac{\partial(xv)}{\partial z} = 0. \tag{3}$$

$$\frac{\partial u}{\partial t} + u\frac{\partial u}{\partial x} + w\frac{\partial u}{\partial z} - \frac{v^2}{x} = \frac{1}{\rho}\frac{\partial}{\partial z}\left(\mu\frac{\partial u}{\partial z}\right) + g(T - T_\infty)\beta\cos\alpha^*, \tag{4}$$

$$\frac{\partial v}{\partial t} + u\frac{\partial v}{\partial x} + w\frac{\partial v}{\partial z} + \frac{uv}{x} = \frac{1}{\rho}\frac{\partial}{\partial z}\left(\mu\frac{\partial v}{\partial z}\right), \tag{5}$$

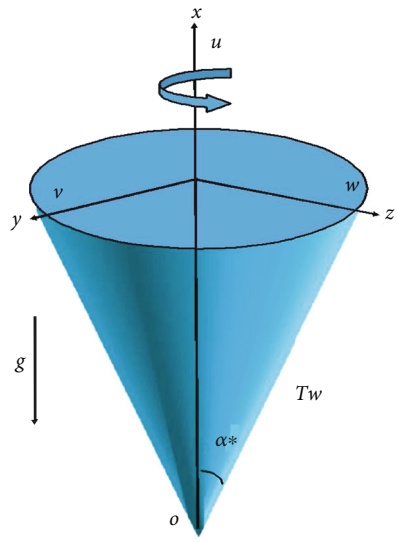


Figure 1: Fluid flow mechanism over a rotating cone.

$$\frac{\partial T}{\partial t} + u\frac{\partial T}{\partial x} + w\frac{\partial T}{\partial z} = \frac{1}{\rho C_p}\frac{\partial}{\partial z}\left(k\frac{\partial T}{\partial z}\right) + \frac{\mu}{\rho C_p}\left[\left(\frac{\partial u}{\partial z}\right)^2 + \left(\frac{\partial v}{\partial z}\right)^2\right]. \tag{6}$$

$$\frac{\partial C}{\partial t} + u\frac{\partial C}{\partial x} + w\frac{\partial C}{\partial z} = D\frac{\partial^2 C}{\partial z^2}. \tag{7}$$

Where $\alpha^*$, $\beta$, $k$, $\rho$, and $g$ are the cone vertical angle, thermal expansion, thermal conductivity, density, and gravity, respectively.

The boundary conditions are:

$$u(0) = 0, v(0) = \frac{1}{(1-st^*)}\Omega x \sin\alpha^*, T(0) = T_w, C(0) = C_w,$$
$$u(\infty) \longrightarrow 0, v(\infty) \longrightarrow 0, T(\infty) \longrightarrow T_\infty, C(\infty) \longrightarrow C_\infty. \tag{8}$$

To simplify the PDEs to ODES, we commence the preceding similarity variables [26]:

$$u = \frac{1}{2(1-st^*)}\Omega x \sin\alpha^* f'(\eta),$$
$$w = \left(\frac{1}{(1-st^*)}\Omega x \sin\alpha^*\right)^{\frac{1}{2}} f(\eta), \eta = \left(\frac{\Omega \sin\alpha^*}{v_0(1-st^*)}\right)^{\frac{1}{2}} z,$$
$$T = T_\infty + (T_w - T_\infty)\theta(\eta), T_w - T_\infty = \frac{(T_0 - T_\infty)}{(1-st^*)^2}\frac{x}{l},$$
$$v = \frac{1}{(1-st^*)}\Omega x \sin\alpha^* g(\eta),$$
$$C = C_\infty + (C_w - C_\infty)\phi(\eta), \text{where } t^* = (\Omega \sin\alpha^*)t, \tag{9}$$

By plunking Equation (9) in Equation (3)–(8), we track down:

Table 1: Comparative analysis with [26] $\alpha = 1$.

| | Ref. [26] | | | Present work | | |
|---|---|---|---|---|---|---|
| $\eta$ | $f''(\eta)$ | $g'(\eta)$ | $\theta'(\eta)$ | $f''(\eta)$ | $g'(\eta)$ | $\theta'(\eta)$ |
| 1.0 | 0.5666 | 1.2994 | 1.5036 | 0.5667 | 1.2996 | 1.5039 |
| 4.0 | 0.6616 | 1.3526 | 1.3883 | 0.6635 | 1.3740 | 1.3911 |
| 8.0 | 0.6633 | 1.3738 | 1.3909 | 0.6642 | 1.3761 | 1.3909 |
| 12 | 0.6642 | 1.3758 | 1.3903 | 0.6645 | 1.3761 | 1.3899 |
| 16 | 0.6645 | 1.3761 | 1.3899 | 0.6645 | 1.3761 | 1.3899 |
| 20 | 0.6645 | 1.3761 | 1.3899 | 0.6645 | 1.3761 | 1.3899 |

Table 2: Comparative analysis between fractional and numerical outcomes.

| Numerical (bvp4c) | | | | Fractional (FDE12) | |
|---|---|---|---|---|---|
| $Pr$ | $\lambda$ | $C_{fx}\mathrm{Re}_x^{1/2}$ | $0.5C_{fy}\mathrm{Re}_x^{1/2}$ | $C_{fx}\mathrm{Re}_x^{1/2}$ | $0.5C_{fy}\mathrm{Re}_x^{1/2}$ |
| | 0 | 1.1254 | 0.7153 | 1.1256 | 0.7155 |
| 1.7 | 1 | 2.3008 | 0.9492 | 2.3009 | 0.9494 |
| | 10 | 8.6042 | 1.4990 | 8.6045 | 1.4993 |
| | 0 | 1.1256 | 0.7157 | 1.1257 | 0.7161 |
| 9 | 1 | 1.5627 | 0.7835 | 1.5630 | 0.7845 |
| | 10 | 5.1821 | 0.9941 | 5.1823 | 0.9950 |

Table 3: Comparative analysis between fractional and numerical outcomes.

| Numerical (bvp4c) | | | | Fractional (FDE12) | |
|---|---|---|---|---|---|
| $Pr$ | $\lambda$ | $Nu\mathrm{Re}_x^{-1/2}$ | $\mathrm{Re}^{-1/2}Sh_r$ | $Nu\mathrm{Re}_x^{-1/2}$ | $\mathrm{Re}^{-1/2}Sh_r$ |
| | 0 | 0.3255 | 0.5276 | 0.3257 | 0.5278 |
| 1.7 | 1 | 0.6121 | 0.7123 | 0.6126 | 0.7127 |
| | 10 | 1.0097 | 1.2099 | 1.0099 | 1.2102 |
| | 0 | 1.4110 | 1.5112 | 1.4121 | 1.5121 |
| 9 | 1 | 1.5660 | 1.6662 | 1.5678 | 1.6671 |
| | 10 | 2.3581 | 2.5583 | 2.3593 | 2.5592 |

$$f'''(1-A\theta) - f''A\theta' + \frac{1}{2}\left(f'\right)^2 - 2g^2 - ff'' - 2\lambda\theta - s\left(\frac{\eta}{2}f'' + f'\right) = 0, \tag{10}$$

$$g''(1-A\theta) - Ag'\theta' + gf' - fg' - s((\eta/2)g' + g) = 0,$$
$$(11)(1/\mathrm{Pr})(\varepsilon(\theta')^2 + (1+\varepsilon\theta)\theta'') - f\theta' + 1/2f'\theta - s((\eta/2)\theta + 2\theta) + Ec((g')^2 + 1/4(f'')^2)(1-A\theta) = 0, \tag{12}$$

$$\left(\phi'' - Sc\left(g\phi'\right)\right) = 0. \tag{11}$$

The reduced conditions are:

$$f(0) = 0, g(0) = 1, f'(0) = \phi(0) = 0, \theta(0) = 0,$$
$$f'(\infty) \longrightarrow 0, g(\infty) \longrightarrow 0, \phi(\infty) \longrightarrow 0, \theta(\infty) \longrightarrow 0, \tag{12}$$

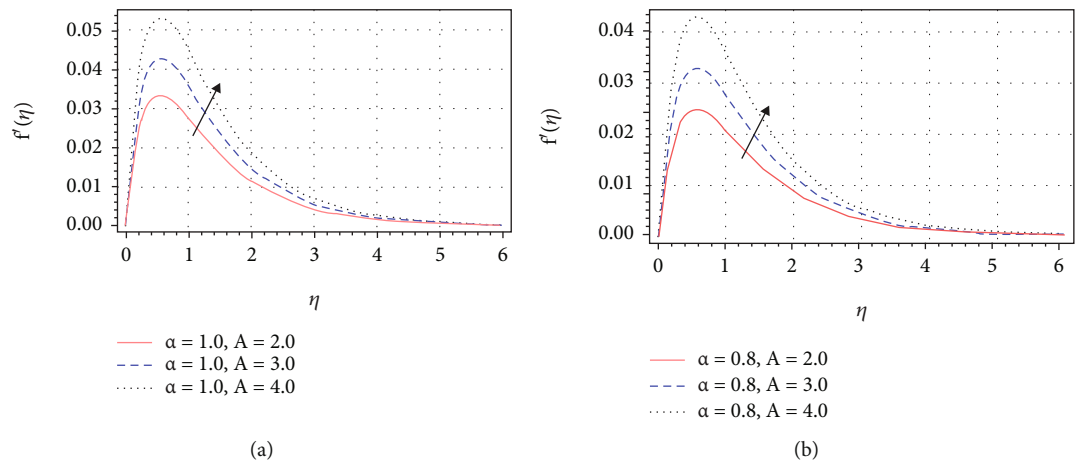


Figure 2: Viscosity parameter $A$ effect on axial velocity profile $f'(\eta)$.

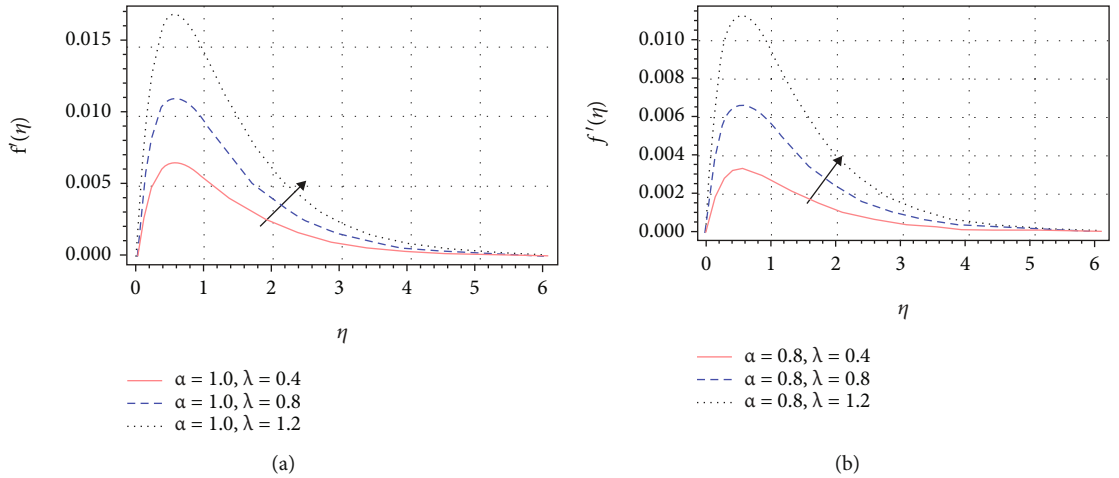


Figure 3: Mixed convection parameter $\lambda$ effect on axial velocity profile $f'(\eta)$.

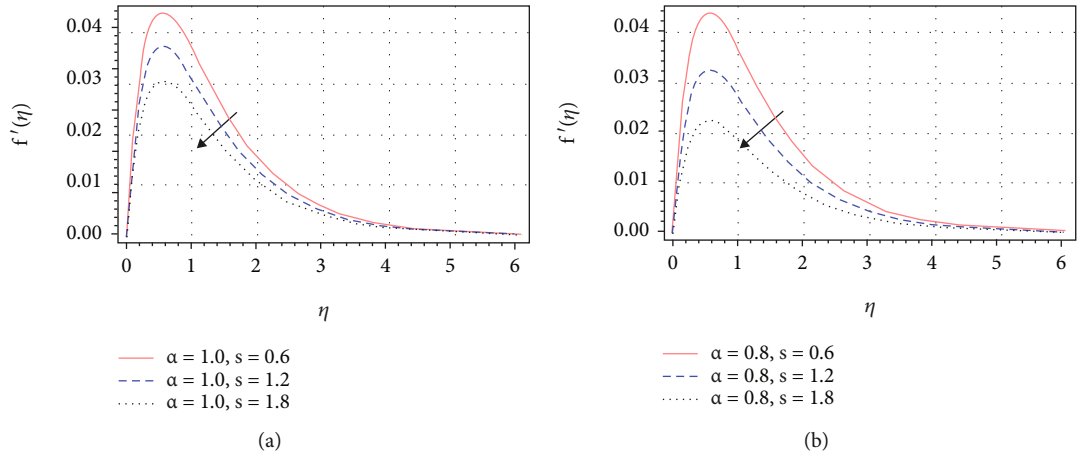


Figure 4: Unsteadiness parameter $S$ effect on axial velocity profile $f'(\eta)$.

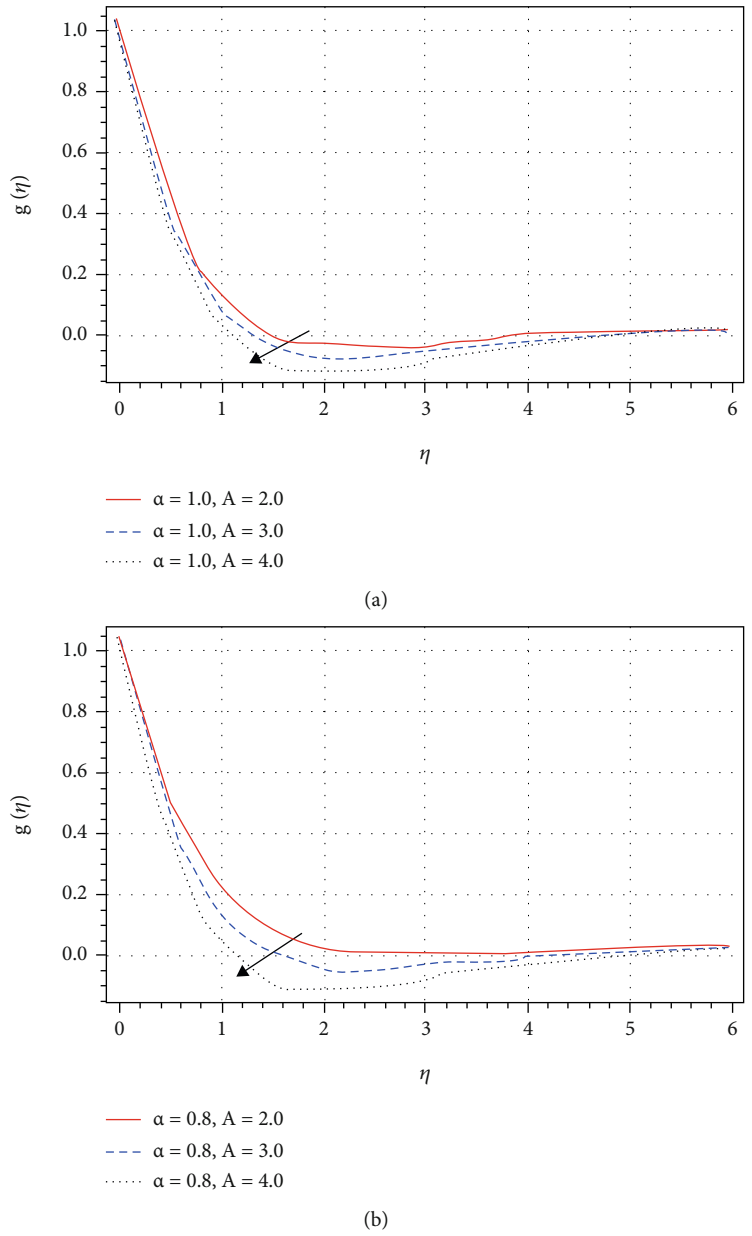


Figure 5: Viscosity parameter $A$ effect on radial velocity profile $g(\eta)$.

The parameters generated are rebound as:

$$\mathrm{Pr} = \frac{\upsilon}{\alpha}, \mathrm{Re}_L = \Omega \sin \alpha^* \frac{L^2}{\nu_0}, Gr = g(T_0 - T_\infty)\frac{L^3}{\nu_0^2}\beta \cos \alpha^*,$$
$$\lambda = \frac{Gr}{\mathrm{Re}_L}, Ec = \frac{xL(\Omega \sin \alpha^*)^2}{C_p(T_0 - T_w)}, Sc = \frac{\upsilon_f}{D_f}. \tag{13}$$

Where Pr, $Sc$, and $Ec$ are the Prandtl, Schmidth, and Eckert number, respectively. While $S$ is the unsteadiness and $\lambda$is the mixed convection coefficient.

The skin friction, mass transfer, and Nusselt number are written as:

$$C_{\mathrm{fx}} = \frac{2\tau_{\mathrm{xz}}|_{z=0}}{\rho[\Omega \sin \alpha^*/(1 - \mathrm{st}^*)]^2}, C_{\mathrm{fy}} = \frac{-2\tau_{\mathrm{yz}}|_{z=0}}{\rho[\Omega \sin \alpha^*/(1 - \mathrm{st}^*)]^2}, \tag{14}$$

$$Sh_r = -\frac{x(\partial C/\partial z)|_{z=0}}{(Cw - C_\infty)}, Nu_x = \frac{x(\partial T/\partial z)|_{z=0}}{(T_w - T_\infty)}. \tag{15}$$

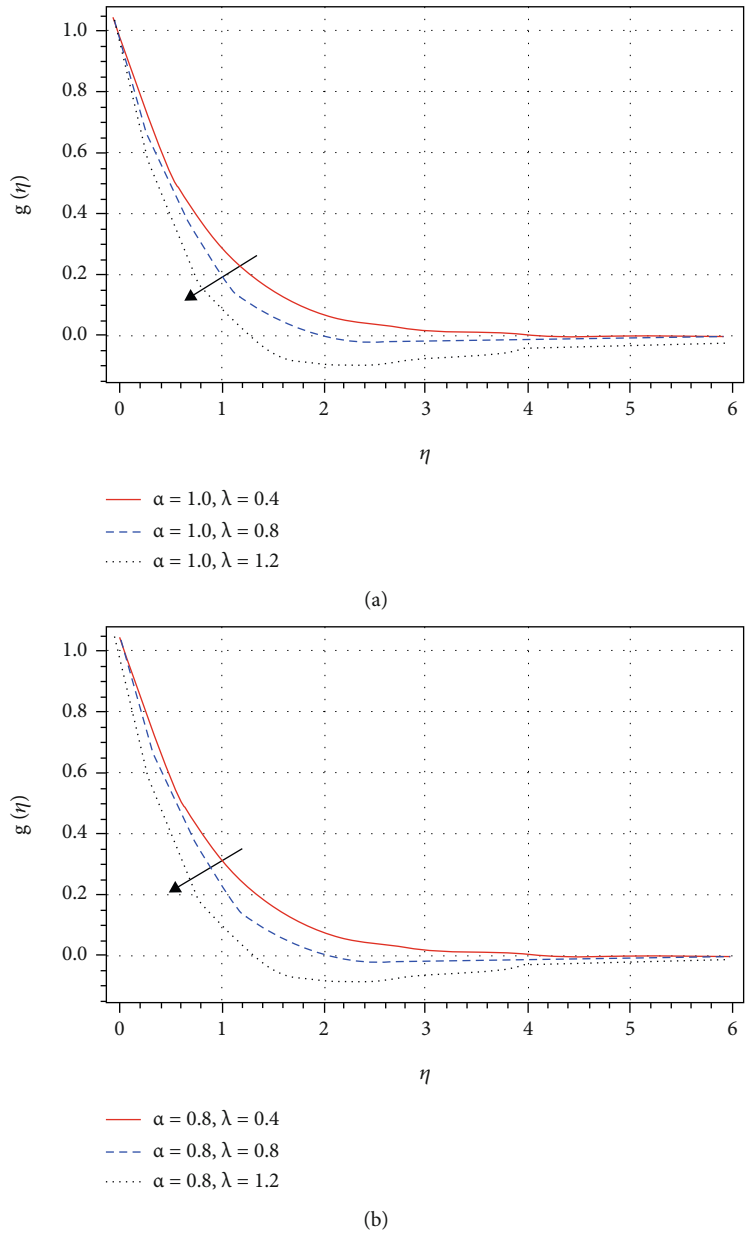


Figure 6: Mixed convection parameter $\lambda$ effect on radial velocity profile $g(\eta)$.

Equations (14) and (15) dimensionless set up are:

$$C_{fx}\,\mathrm{Re}_x^{\frac{1}{2}} = \left[-(1-A\theta)f''(\eta)\right]_{\eta=0},$$
$$C_{fy}\,\mathrm{Re}_x^{\frac{1}{2}} = \left[-(1-A\theta)g'(\eta)\right]_{\eta=0},$$

$$Nu_x\,\mathrm{Re}_x^{-1/2} = -\theta'(\eta)_{\eta=0}, \mathrm{Re}^{-1/2}Sh_r = -\phi'(0). \tag{16}$$

Where

$$\mathrm{Re}_x = \frac{1}{\nu_0(1-st^*)}\Omega x^2 \sin\alpha^*. \tag{17}$$

## 3. Preliminaries

*Definition 1.* For a function $g:\Re^+ \longrightarrow \Re$, the fractional integral of order $\alpha > 0$ is defined as:

$$I_t^\alpha(g(t)) = \frac{1}{\Gamma(\alpha)}\int (t-\chi)^{\alpha-1}g(\chi)d\chi. \tag{18}$$

*Definition 2.* For function $g \in C^n$, the Caputo noninteger order derivative is defined as:

$${}^cD_t^\alpha(g(t)) = I^{n-\alpha}D^n g(t) = \frac{1}{\Gamma(n-\alpha)}\int_0^t \frac{g^n(\chi)}{(t-\chi)^{\alpha+n-1}}d\chi. \tag{19}$$

Clearly ${}^cD_t^\alpha(g(t))$ tends to $g'(t)$ as $\alpha \longrightarrow 1$.

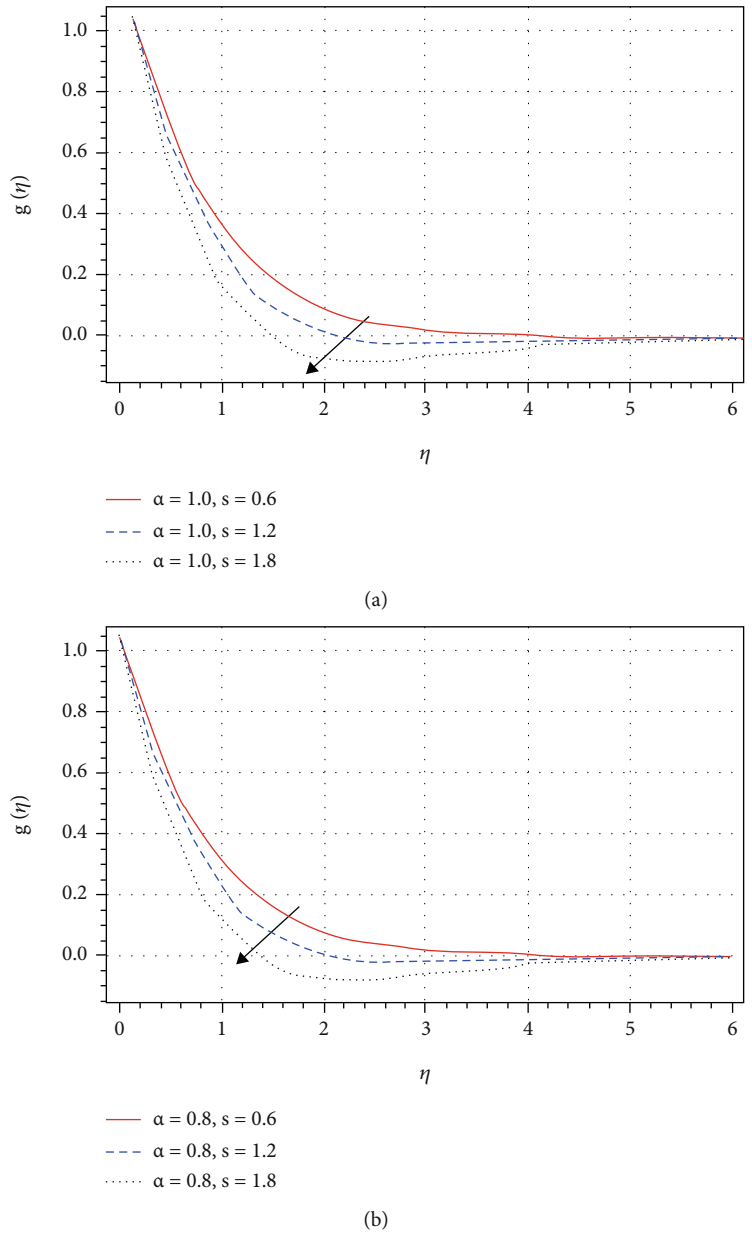


FIGURE 7: Unsteadiness parameter $S$ effect on radial velocity profile $g(\eta)$.

## 4. Problem Solution

By defining the preceding variables, the system of ODEs (10))–(13) and (14) are reduced to a dimensionless first order differential equations (DE):

$$\eta = \gamma_1, f = \gamma_2, f' = \gamma_3, f'' = \gamma_4, g = \gamma_5, g' = \gamma_6, \theta = \gamma_7, \theta' = \gamma_8, \phi = \gamma_9, \phi' = \gamma_{10}.\Big\}$$

$$\begin{cases} \gamma_1 = 1, \gamma_2 = \gamma_3, \gamma_3 = \gamma_4 \\ \gamma_4 = \dfrac{1}{1 - A\gamma_7}\left\{A\gamma_8\gamma_4 - \dfrac{1}{2}(\gamma_3)^2 + \gamma_2\gamma_4 + 2(\gamma_5)^2 + 2\lambda\gamma_7 + S\left(\gamma_3 + \dfrac{\eta}{2}\gamma_4\right)\right\}, \\ \gamma_5 = \gamma_6, D_t^{\alpha}\gamma_6 = \dfrac{1}{1 - A\gamma_7}\left\{A\gamma_8\gamma_6 + \gamma_2\gamma_6 - \gamma_5\gamma_3 + S\left(\gamma_5 + \dfrac{\eta}{2}\gamma_6\right)\right\}, \gamma_7 = \gamma_{8,} \\ \gamma_8 = \dfrac{1}{1 + \varepsilon\gamma_7}\left\{\Pr\left[\gamma_2\gamma_8 - \dfrac{1}{2}\gamma_3\gamma_7 + S\left(\dfrac{\eta}{2}\gamma_7 + 2\gamma_7\right) - Ec\left(\dfrac{1}{4}(\gamma_4)^2 + (\gamma_6)^2\right)(1 - A\gamma_7)\right] - \varepsilon(\gamma_8)^2\right\}, \\ \gamma_9 = \gamma_{10,}\gamma_{10} = Sc(\gamma_5\gamma_{10}). \end{cases} \tag{20}$$

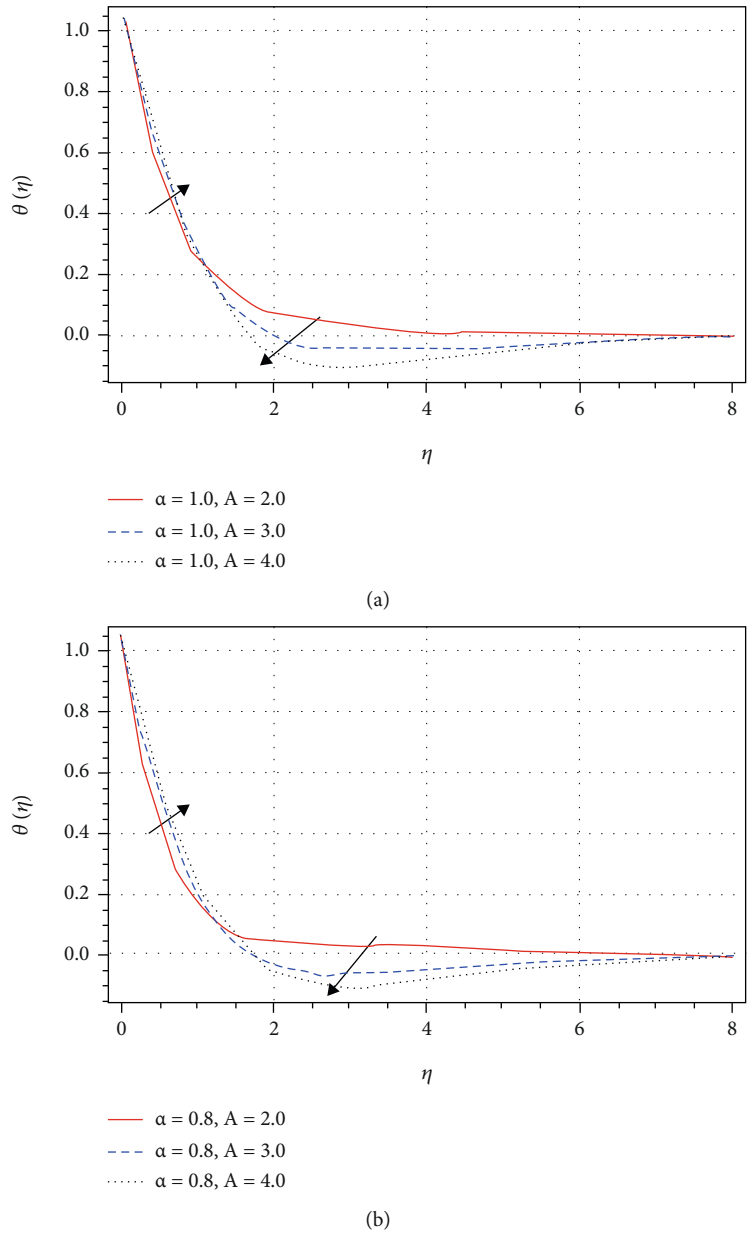


FIGURE 8: Viscosity parameter $A$ effect on energy profile $\theta(\eta)$.

We now use the Caputo fractional derivative to extend the previous system of first order DEs to noninteger order:

$$\begin{cases} D_t^{\alpha}\gamma_4 = \dfrac{1}{1-A\gamma_7}\left\{A\gamma_8\gamma_4 - \dfrac{1}{2}(\gamma_3)^2 + \gamma_2\gamma_4 + 2\lambda\gamma_7 + 2(\gamma_5)^2 + S\left(\dfrac{\eta}{2}\gamma_4 + \gamma_3\right)\right\}, \\ D_t^{\alpha}\gamma_6 = \dfrac{1}{1-A\gamma_7}\left\{A\gamma_8\gamma_6 - \gamma_5\gamma_3 + \gamma_2\gamma_6 + S\left(\dfrac{\eta}{2}\gamma_6 + \gamma_5\right)\right\}, D_t^{\alpha}\gamma_{10} = Sc(\gamma_{10}\gamma_5), \\ D_t^{\alpha}\gamma_8 = \dfrac{1}{1+\varepsilon\gamma_7}\left\{\Pr\left[\gamma_8\gamma_2 - \dfrac{1}{2}\gamma_3\gamma_7 + S\left(\dfrac{\eta}{2}\gamma_7 + 2\gamma_7\right) - Ec\left((\gamma_6)^2 + \dfrac{1}{4}(\gamma_4)^2\right)(1-A\gamma_7)\right] - \varepsilon(\gamma_8)^2\right\}. \end{cases} \tag{21}$$

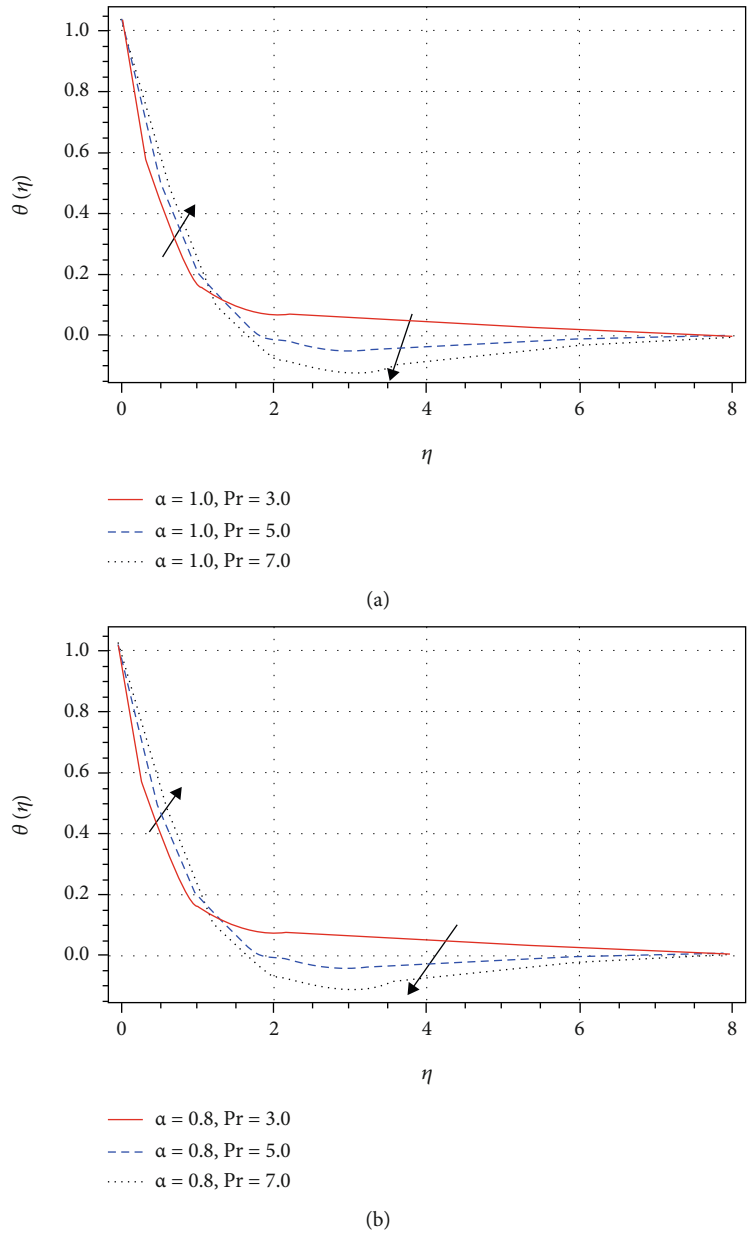


FIGURE 9: Prandtl number Pr effect on enery profile $\theta(\eta)$.

## 5. Result and Discussion

The purpose of this section is to quantify and compare the functionality of energy and mass transition rate based on various physical factors. The findings are produced using Matlab fractional package (fde12), and a fast-approaching numerical technique bvp4c, has been applied to ensure the validity and correctness of the outcomes.

Table 1 shows the adequacy of the current study when compared to [26]. While the fractional and numerical methods have been compared in Tables 2 and 3, respectively. For mixed convection and Prandtl number Pr, the numerical outcomes of tangential and azimuthal skin friction is shown in Table 2. For mixed convection and Prandtl number, Table 3 shows the quantitative results of Sherwood Nusselt number.

The schematic drawing of a revolving cone is depicted in Figure 1. Figures 2–12(a) depict the behavior of various flow entities when $\alpha = 1$, whereas Figures 2–12(b) describe the fractional behavior of basic constraints when $\alpha = 0.8$.

The upshot of $A$ (variable viscosity) on the velocity field is noticed in Figure 2. At $t = 0$, the velocity at the cone surface is assumed to be zero, and with increasing credit of viscosity variation, the fluid velocity rises in both Figures 2(a) and 2(b).

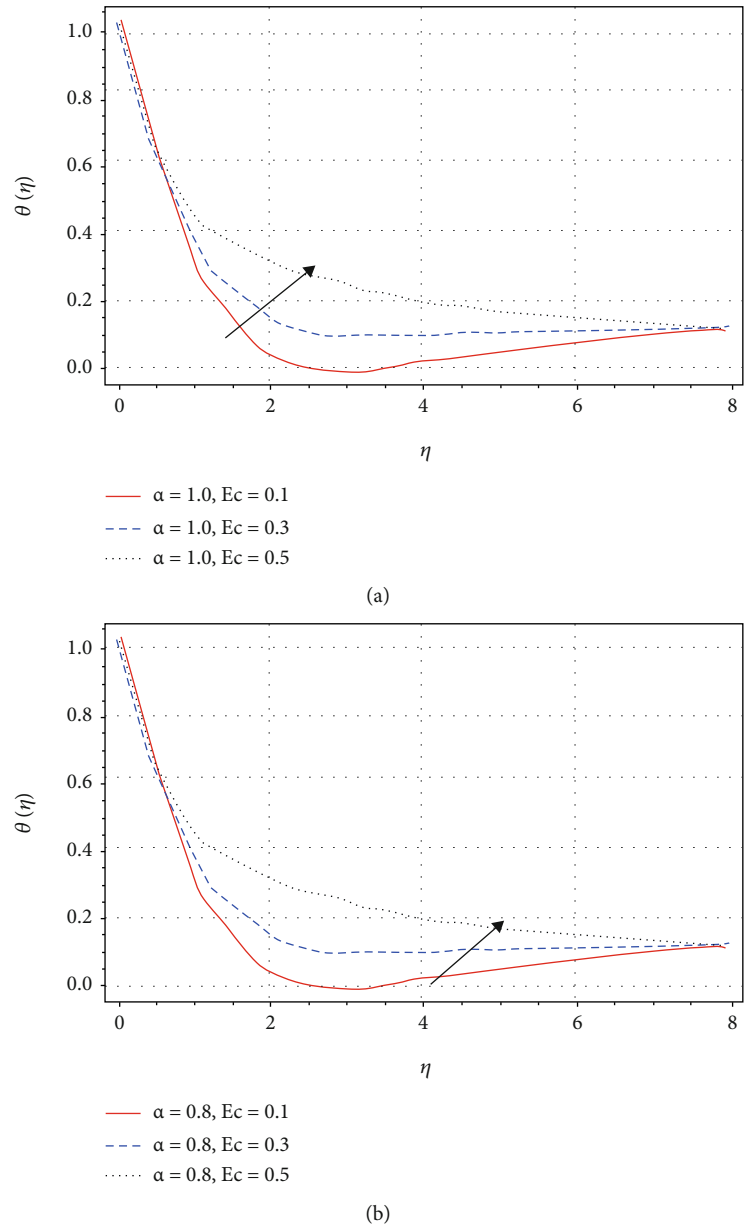


FIGURE 10: Eckert number $Ec$ effect on energy profile $\theta(\eta)$.

Figures 3(a) and 3(b) demonstrate the distribution of the mixed convection $\lambda$ vs the axial velocity profile $f'(\eta)$. Physically, mixed convection has a beneficial influence on boundary layer thickness, resulting in an increase in fluid axial velocity. Convection decreases fluid density, causing fluid particles to move as a result of forces and pressure.

Figures 4(a) and 4(b) show that increasing the value of the unsteadiness parameter $S$ lowers fluid velocity. Figures 5(a) and 5(b) exhibit the radial velocity features versus the variable viscosity coefficient $A$. It has been discovered that when the variable viscosity $A$ increases, the fluid's radial velocity decreases. Figures 6(a) and 6(b) depict the effect of the convection component on radial velocity. The convection component has a significant impact on fluid motion, and as a result, the velocity drops. In the presence of the unsteadiness parameter $S$, the radial velocity responds similar as an axial velocity. The radial velocity decreases with the increment in $S$ as elaborated through Figures 7(a) and 7(b).

Figures 8(a) and 8(b) show a reduction in thermal gradient when the variable viscosity factor is increased. The interaction forces within fluid molecules grow as the amount of variable viscosity rises, which results in the lowering fluid energy profile. It is self-evident that when the Prandtl number Pr increases, the fluid temperature significantly reduces. Because a fluid with a higher Prandtl number has a lower thermal diffusivity (Figures 9(a) and 9(b)).

In Figures 10(a) and 10(b), an increase in energy profile is observed against the Eckert number $Ec$. The Eckert number describes a fluid's self-rising thermal rate as a result of

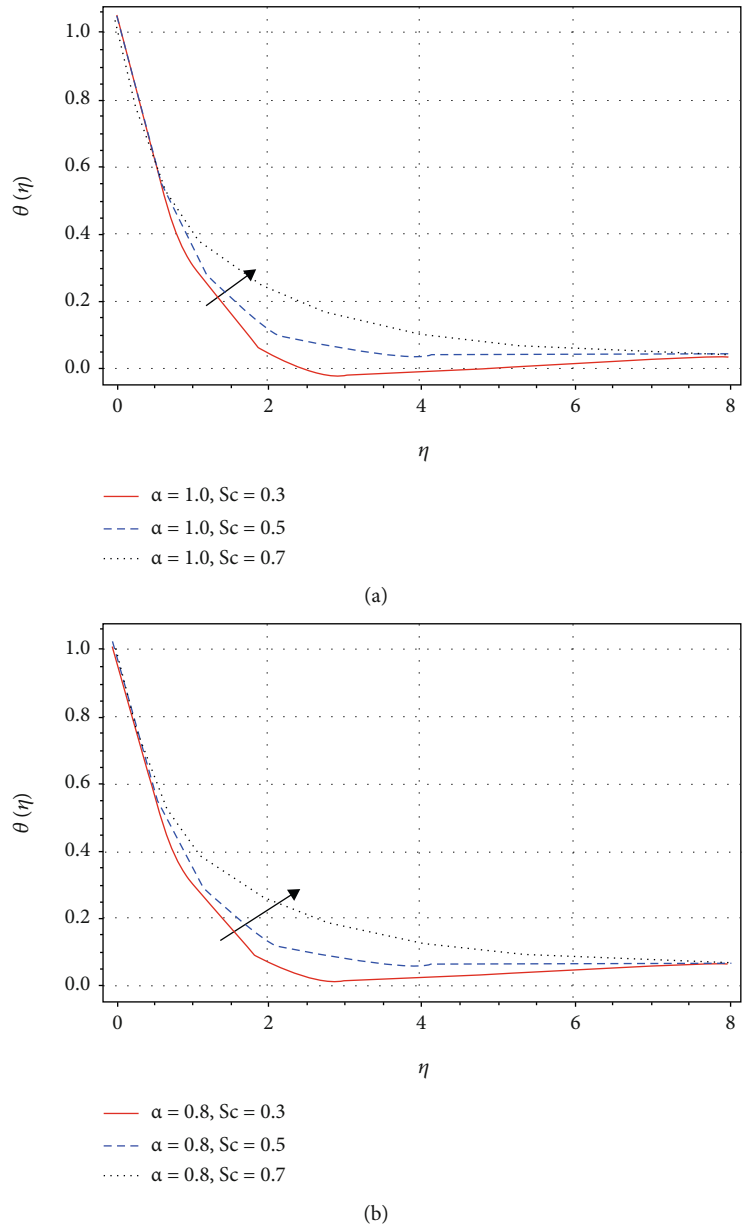


FIGURE 11: Variable thermal conductivity $\varepsilon$ effect on energy profile $\theta(\eta)$.

viscous dissipation. The fluid temperature is efficiently increased using a variable thermal conductivity as revealed through Figures 11(a) and 11(b). The result of Schmidt number vs mass transmission rate is shown in Figures 12(a) and 12(b). The fluid's mass transfer rate is reduced as the Schmidt number is increased.

## 6. Conclusion

The rotating flow of a viscous fluid with time-dependent viscosity and thermal conductivity across a vertical cone is evaluated in this study. A comparison of the numerical bvp4c method and fractional fde12 package is also emphasized. The study's compelling observations are listed below:

(i) With a positive increase in unsteadiness entity $S$, both the axial and radial velocity declines

(ii) As the value of the mixed convection component improves, the fluid axial velocity $f'(\eta)$ appears to increase substantially, but the secondary velocity $g(\eta)$ gradient decreases

(iii) Similarly, the main velocity $f'(\eta)$ increases as the viscosity variability component A grows, while the radial velocity $g(\eta)$ operates transversely as $A$ increases

(iv) Improvements in thermal conductivity, Eckert number Ec and viscosity constraint A, limit the rate of thermal energy transference $Nu\mathrm{Re}_x^{-1/2}$

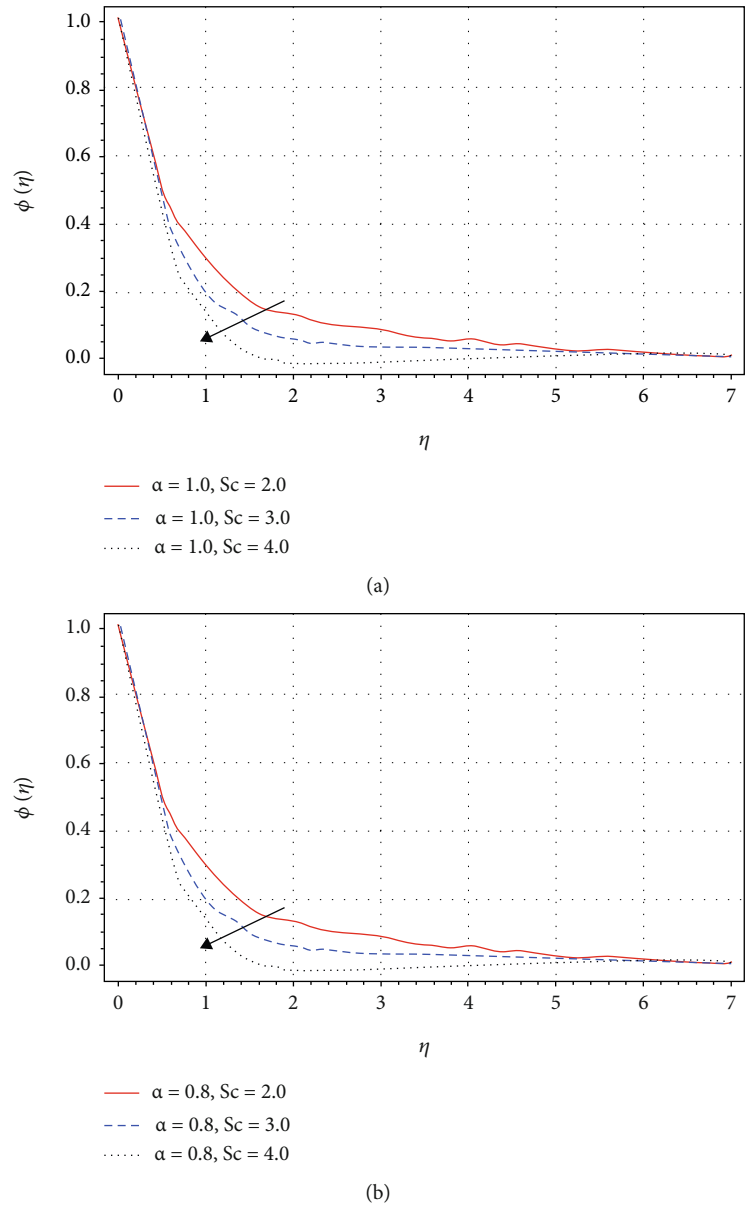


Figure 12: Schmidth number effect on mass profile $\phi(\eta)$.

(v) Mixed convection has a beneficial influence on boundary layer thickness, resulting in an increase in fluid primary velocity. Convection reduces the density of the fluid, causing fluid particles to flow owing to forces and pressure

## Nomenclature

$S$: Unsteadiness parameter
$\alpha^*$: Semi vertical angle of cone
$T$: Fluid temperature (K)
$T_\infty$: Temperature away from cone surface
$\varepsilon$: Variable thermal conductivity coefficient
$\eta$: Similarity variable
$\mu_0$: Dynamic viscosity
$\nu_0$: Kinematic viscosity
$Pr$: Prandtl number
$\theta$: Dimensionless temperature
$\rho$: Density
$c_p$: Specific heat
$z$-axis: Axial or normal to cone
$C_{fx}$: Skin friction
$Nu_x$: Nusselt number
*Bvp4c*: Boundary value solver
$u, v, w$: Velocity component
$\alpha$: Fractional order
$T_w$: Wall temperature
$\beta$: Temperature expansion coefficient
$g$: Gravity
$\lambda$: Mixed convection
$t^*$: Dimensionless time
$k$: Thermal conductivity

$\Omega$: Angular velocity of disk ($\mathrm{r\,s^{-1}}$)
$\phi$: Dimensionless concentration
$k_0$: Fluid conductivity
$Ec$: Eckert number
$A$: Variable viscosity coefficient
$C_{fy}$: Skin friction
$Sh_x$: Sherwood number
FDE12: Matlab fractional package.

## Data Availability

All the data exist in the manuscript.

## Conflicts of Interest

The authors declare that they have no conflicts of interest.

## Acknowledgments

The authors extend their appreciation to the Deanship of Scientific Research at King Khalid University for funding this work through research groups under grant number R.G.P.1/154/42.

## References

[1] C. Spruell and A. B. Baker, "Analysis of a high-throughput cone-and-plate apparatus for the application of defined spatio-temporal flow to cultured cells," *Biotechnology and Bioengineering*, vol. 110, no. 6, pp. 1782–1793, 2013.

[2] M. Turkyilmazoglu, "On the purely analytic computation of laminar boundary layer flow over a rotating cone," *International Journal of Engineering Science*, vol. 47, no. 9, pp. 875–882, 2009.

[3] A. J. Chamkha and A. Al-Mudhaf, "Unsteady heat and mass transfer from a rotating vertical cone with a magnetic field and heat generation or absorption effects," *International Journal of Thermal Sciences*, vol. 44, no. 3, pp. 267–276, 2005.

[4] S. J. Garrett, Z. Hussain, and S. O. Stephen, "Boundary-layer transition on broad cones rotating in an imposed axial flow," *AIAA Journal*, vol. 48, no. 6, pp. 1184–1194, 2010.

[5] S. Nadeem and S. Saleem, "Theoretical investigation of MHD nanofluid flow over a rotating cone: An optimal solutions," *Information Sciences Letters*, vol. 3, no. 2, pp. 55–62, 2014.

[6] P. D. Towers and S. J. Garrett, "Similarity solutions of compressible flow over a rotating cone with surface suction," *Thermal Science*, vol. 20, no. 2, pp. 517–528, 2016.

[7] T. Hayat, S. A. Khan, M. I. Khan, and A. Alsaedi, "Irreversibility characterization and investigation of mixed convective reactive flow over a rotating cone," *Computer Methods and Programs in Biomedicine*, vol. 185, no. 185, article 105168, 2020.

[8] A. J. Chamkha, F. Selimefendigil, and H. F. Oztop, "Effects of a rotating cone on the mixed convection in a double lid-driven 3D porous trapezoidal nanofluid filled cavity under the impact of magnetic field," *Nanomaterials*, vol. 10, no. 3, p. 449, 2020.

[9] Massoudi and Christie, "Effects of variable viscosity and viscous dissipation on the flow of a third grade fluid in a pipe," *International Journal of Non-Linear Mechanics*, vol. 30, no. 5, pp. 687–699, 1995.

[10] M. A. Seddeek, "Effects of radiation and variable viscosity on a MHD free convection flow past a semi-infinite flat plate with an aligned magnetic field in the case of unsteady flow," *International Journal of Heat and Mass Transfer*, vol. 45, no. 4, pp. 931–935, 2002.

[11] A. Pantokratoras, "Study of MHD boundary layer flow over a heated stretching sheet with variable viscosity: a numerical reinvestigation," *International Journal of Heat and Mass Transfer*, vol. 51, no. 1-2, pp. 104–110, 2008.

[12] S. Mukhopadhyay and G. C. Layek, "Effects of thermal radiation and variable fluid viscosity on free convective flow and heat transfer past a porous stretching surface," *International Journal of Heat and Mass Transfer*, vol. 51, no. 9-10, pp. 2167–2178, 2008.

[13] M. S. Dada and C. Onwubuoya, "Variable viscosity and thermal conductivity effects on Williamson fluid flow over a slendering stretching sheet," *Journal of Engineering*, vol. 17, no. 3, 371 pages, 2020.

[14] G. C. Hazarika, B. Phukan, and S. Ahmed, "Effect of variable viscosity and thermal conductivity on unsteady free convective flow of a micropolar fluid past a vertical cone," *Journal of Engineering Physics and Thermophysics*, vol. 93, no. 1, pp. 178–185, 2020.

[15] M. G. Reddy, P. Padma, and S. Bandari, "Effects of viscous dissipation and heat source on unsteady MHD flow over a stretching sheet," *Ain Shams Engineering Journal*, vol. 6, no. 4, pp. 1195–1201, 2015.

[16] F. Mabood, S. Shateyi, M. M. Rashidi, E. Momoniat, and N. Freidoonimehr, "MHD stagnation point flow heat and mass transfer of nanofluids in porous medium with radiation, viscous dissipation and chemical reaction," *Advanced Powder Technology*, vol. 27, no. 2, pp. 742–749, 2016.

[17] W. Deebani, A. Tassaddiq, Z. Shah, A. Dawar, and F. Ali, "Hall effect on radiative casson fluid flow with chemical reaction on a rotating cone through entropy optimization," *Entropy*, vol. 22, no. 4, p. 480, 2020.

[18] M. Gayatri, K. J. Reddy, and M. J. Babu, "Slip flow of Carreau fluid over a slendering stretching sheet with viscous dissipation and Joule heating," *SN Applied Sciences*, vol. 2, no. 3, pp. 1–1, 2020.

[19] S. Murtaza, M. Iftekhar, F. Ali, and I. Khan, "Exact analysis of non-linear Electro-Osmotic flow of generalized maxwell nanofluid: applications in concrete based nano-materials," *IEEE Access*, vol. 8, no. 8, pp. 96738–96747, 2020.

[20] A. A. A. Kilbas, H. M. Srivastava, and J. J. Trujillo, *Theory and Applications of Fractional Differential Equations*, vol. 204, Elsevier Science Limited, 2006.

[21] F. Mainardi, *Fractional Calculus and Waves in Linear Viscoelasticity: An Introduction to Mathematical Models*, World Scientific, 2010.

[22] Z. M. Odibat, "Computing eigenelements of boundary value problems with fractional derivatives," *Mathematics of Computation*, vol. 215, no. 8, pp. 3017–3028, 2009.

[23] M. Caputo and M. Fabrizio, "A new definition of fractional derivative without singular kernel," *Progress in Fractional Differentiation and Applications*, vol. 1, no. 2, pp. 1–13, 2016.

[24] M. Ahmad, J. Jiang, A. Zada, S. O. Shah, and J. Xu, "Analysis of coupled system of implicit fractional differential equations involving Katugampola–Caputo fractional derivative," *Complexity*, vol. 2020, 11 pages, 2020.

[25] Y. X. Li, T. Muhammad, M. Bilal, M. A. Khan, A. Ahmadian, and B. A. Pansera, "Fractional simulation for Darcy-Forchheimer hybrid nanoliquid flow with partial slip over a spinning disk," *Alexandria Engineering Journal*, vol. 60, no. 5, pp. 4787–4796, 2021.

[26] M. Y. Malik, H. Jamil, T. Salahuddin, S. Bilal, K. U. Rehman, and Z. Mustafa, "Mixed convection dissipative viscous fluid flow over a rotating cone by way of variable viscosity and thermal conductivity," *Results in Physics*, vol. 6, no. 6, pp. 1126–1135, 2016.